

Nematic quantum phases in the bilayer honeycomb antiferromagnet

Hao Zhang,^{1,*} C. A. Lamas,^{2,†} M. Arlego,² and Wolfram Brenig^{3,‡}

¹State Key Laboratory of Optoelectronic Materials and Technologies, School of Physics, Sun Yat-Sen University, Guangzhou 510275, China

²IFLP-CONICET, Departamento de Física, Universidad Nacional de La Plata, Casilla de Correo 67, 1900 La Plata, Argentina

³Institute for Theoretical Physics, Technical University Braunschweig, D-38106 Braunschweig, Germany



(Received 22 December 2017; published 14 June 2018)

The spin-1/2 Heisenberg antiferromagnet on the honeycomb bilayer lattice is shown to display a rich variety of semiclassical and genuinely quantum phases, controlled by the interplay between intralayer frustration and interlayer exchange. Employing a complementary set of techniques, comprising spin rotationally invariant Schwinger boson mean-field theory, bond operators, and series expansions, we unveil the quantum phase diagram, analyzing low-energy excitations and order parameters. By virtue of Schwinger bosons we scan the complete range of exchange parameters, covering both long-range-ordered and quantum disordered ground states, and reveal the existence of an extended, frustration-induced lattice nematic phase in a range of intermediate exchange unexplored so far.

DOI: [10.1103/PhysRevB.97.235123](https://doi.org/10.1103/PhysRevB.97.235123)

I. INTRODUCTION

Frustrated magnets are of great interest to a broad range of subfields in physics, harboring new quantum states of condensed matter [1,2], fueling progress on fundamental paradigms of topological ordering [3–5], providing realistic prospects for quantum computing [6–8] and devices for thermal management technologies [9,10], inspiring research on ultracold atomic gases [11,12], realizing elementary excitations related to grand unified theories [13–15], and exhibiting correlations found in soft matter, liquid crystals, and even cosmic strings [16,17]. Strong frustration in quantum magnets can ultimately lead to spin liquids, free of any broken symmetries, featuring long-range entanglement, topological order, and anyonic excitations [2,18]. Proximate to such liquids, a rich variety of additional exotic quantum matter, including valence-bond crystals, also called *lattice nematics* [19], chiral liquids [20], multipolar states [21], and more complex phases compete for stability. Understanding such phases of matter and their interplay is a critical outstanding problem for theory and experiment. In this paper we take a major step forward in this direction and detail the emergence of lattice nematic order in an as yet unexplored region of frustrated magnets on bilayer honeycomb lattices.

Recently, frustrated Heisenberg models on single-layer honeycomb lattices have become a test bed for competing spiral order, lattice nematicity, and plaquette valence-bond states [22–39]. This interest has been propelled by the discovery of bismuth oxynitrate, $\text{Bi}_3\text{Mn}_4\text{O}_{12}(\text{NO}_3)$ [40], where Mn^{4+} ions of spin 3/2 form honeycomb layers, with both nearest- and next-nearest-neighbor antiferromagnetic (AFM) exchange. Early on, however, it was noticed that in this compound Mn^{4+} ions are grouped into pairs along the c axis, rendering the structure rather that of a bilayer honeycomb

lattice. Despite a significant separation through bismuth atoms, density functional calculation [41] resulted in comparable inter- and intralayer exchanges, consistent with experimental findings [42]. This has led to investigations of bilayer honeycomb systems [43–49]. Most of these studies have focused on the stability of the semiclassical phases, extending previous work on the single-layer case.

The first indications of quantum disordered phases genuinely related to the bilayer geometry and not present in the single-layer case were provided in a small parameter window in [47], following ideas of [50,51] and similar works [52–56]. However, a complete understanding of the quantum phase diagram of the bilayer is missing, which critically hinders progress in understanding frustrated multilayer quantum magnets in general. Therefore, in this paper we provide a comprehensive analysis of the quantum phases of the frustrated Heisenberg model on the honeycomb bilayer over a wide range of coupling strengths, including, in particular, the intermediate regime, where both the interlayer exchange and intralayer frustration are comparable to the intralayer first-neighbor couplings. This part of the phase diagram has remained largely unexplored, representing a challenge for most of the existing state-of-the-art numerical techniques. Here, by means of a combination of methods, among which Schwinger bosons stand out for their ability to explore the full quantum phase diagram and to treat on equal footing quantum and semiclassical states, we unveil a rich structure of phases, where the interplay of frustration and interlayer coupling is most essential, destroying magnetic order and giving rise to exotic phases. Most noteworthy, we will provide evidence for a lattice nematic phase in the intermediate-coupling regime.

II. THE MODEL AND ITS PHASE DIAGRAM

The model we consider is shown in Fig. 1. Its Hamiltonian reads

$$H = \sum_{\vec{r}, i, l, m} J_i^{(l, m)} \vec{S}_l(\vec{r}) \cdot \vec{S}_m(\vec{r} + \vec{e}_i), \quad (1)$$

*zhanghao25@mail.sysu.edu.cn

†lamas@fisica.unlp.edu.ar

‡w.brenig@tu-bs.de

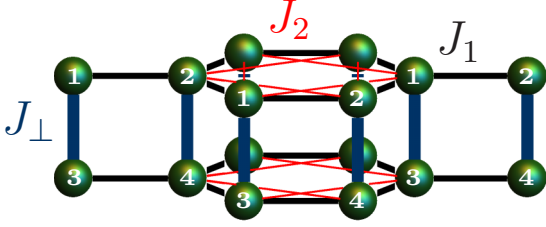


FIG. 1. Schematic representation of the model. The sites (green spheres) in each unit cell are labeled from 1 to 4. Thick vertical blue lines indicate J_\perp interlayer couplings, whereas thin black and red lines indicate J_1 and J_2 first- and second-nearest neighbors, respectively.

where \vec{r} is the position of the unit cell, \vec{e}_i are the primitive vectors of the triangular Bravais lattice, and l, m correspond to the internal label for each site in the unit cell. $\vec{S}_l(\vec{r})$ are spin operators at basis sites $\vec{r}, l = 1, \dots, 4$ of the bilayer. The couplings $J_i^{(l,m)}$ are nonzero, with values J_\perp, J_1 , and J_2 as depicted in Fig. 1.

Before describing our calculations, we focus on the main results, summarized in Fig. 2(a). On the classical level, $S \rightarrow \infty$, and in the single-plane limit, i.e., at $J_\perp = 0$, there are two phases: Néel order for $J_2/J_1 < 1/6$ and spiral order for $J_2/J_1 > 1/6$. Allowing for interlayer coupling this single transition point extends into a line, *independent* of J_\perp . Quantum fluctuations lead to new nonclassical intermediate phases and renormalize the Néel and spiral phases. Previous studies [38] have identified continuous transitions into two frustration-induced genuine quantum phases: a gapped spin liquid (GSL) phase, preserving all lattice symmetries for $0.2075 \lesssim J_2/J_1 \lesssim 0.3732$, and a staggered-dimer lattice nematic phase (VBC1) which maintains the SU(2) spin rotational and lattice translational symmetries but breaks Z_3 symmetry, corresponding to $2\pi/3$ rotations around an axis perpendicular to the plane for $0.3732 \lesssim J_2/J_1 \lesssim 0.398$. Another limiting case is $J_\perp \rightarrow \infty$. Here, an interlayer dimer product phase (IDP) is formed.

Connecting these two limits, the interplay between the interlayer couplings J_\perp and the frustration J_2 reveals the complex phase diagram we find in Fig. 2(a). Starting from the limit of decoupled planes, we consider the semiclassical Néel and spiral phases first. Figure 2(a) shows that small interlayer couplings extend each of their windows of stability along the J_2 direction, even leading to a region of competition. However, for sufficiently large J_\perp the semiclassical phases recess and are suppressed in favor of the IDP. Regarding the GSL and VBC1 phases, interlayer coupling has a dramatic consequence, suppressing them very rapidly, reentering semiclassical phases at finite J_\perp . Finally, the Néel-to-IDP transition is direct. That is not so for the spiral-to-IDP transition. In fact we find yet another lattice nematic region (VBC2) which intervenes. To the best of our knowledge, this has not been observed before.

Next, we detail how to arrive at our main result, i.e., Fig. 2, using three complementary techniques, namely, Schwinger boson mean-field theory (SBMFT) [26], Bond operators (BOs) [57], and series expansions (SEs) [58]. While being a mean-field approach, primarily gauged towards bosonic

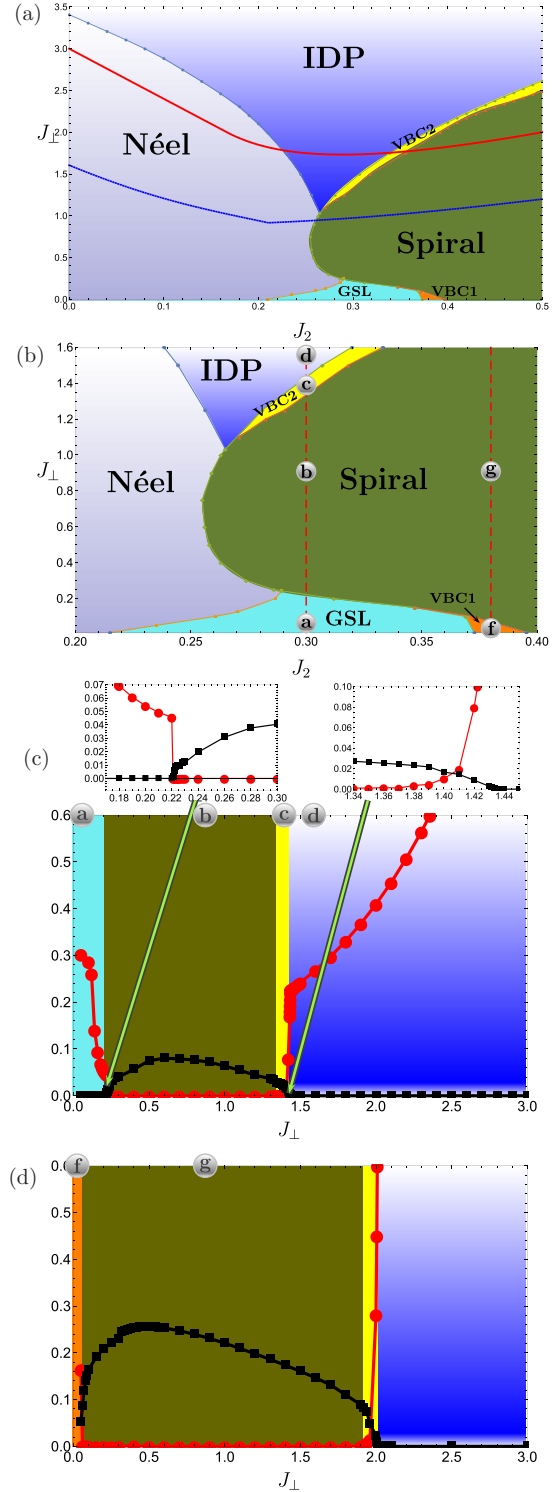


FIG. 2. (a) The different colored regions identify the phases of model (1) in the J_2 - J_\perp plane (in units of J_1) determined by SBMFT. The blue and red lines represent the border of the IDP phase predicted by SE and BO, respectively. (b) Zoom of the phase diagram where two paths along J_\perp for $J_2 = 0.3$ and $J_2 = 0.38$ are indicated with red dashed lines. (c) and (d) The evolution of the gap (connected red circles) and the Z_3 directional symmetry-breaking order parameter ρ (connected black squares) along the mentioned paths.

fixed-point models, SBMFT is superior in addressing on equal footing both semiclassical and genuinely quantum phases, allowing us to scan all of the parameter space of Eq. (1). The other two methods are best suited to obtaining additional information for large interlayer coupling (BO) and for weak frustration (SE).

III. SCHWINGER BOSON MEAN-FIELD THEORY

Here, spin operators are represented by two bosons [59–61],

$$\vec{S}_l(\vec{r}) = \frac{1}{2} \vec{b}_l^\dagger(\vec{r}) \cdot \vec{\sigma} \cdot \vec{b}_l(\vec{r}),$$

where $\vec{b}_l^\dagger(\vec{r}) = (\mathbf{b}_{l,\uparrow}^\dagger(\vec{r}), \mathbf{b}_{l,\downarrow}^\dagger(\vec{r}))$ is a spinor, $\vec{\sigma}$ are the Pauli matrices, and

$$\sum_{\sigma} \mathbf{b}_{l,\sigma}^\dagger(\vec{r}) \mathbf{b}_{l,\sigma}(\vec{r}) = 2S$$

is a local constraint. Using the rotationally invariant representation [26,30,38,62–67], we define two SU(2) invariants,

$$\mathbf{A}_{lm}(\vec{x}, \vec{y}) = \frac{1}{2} \sum_{\sigma} \sigma \mathbf{b}_{l,\sigma}(\vec{x}) \mathbf{b}_{m,-\sigma}(\vec{y})$$

and

$$\mathbf{B}_{lm}(\vec{x}, \vec{y}) = \frac{1}{2} \sum_{\sigma} \mathbf{b}_{l,\sigma}^\dagger(\vec{x}) \mathbf{b}_{m,-\sigma}(\vec{y}),$$

where the former generates a spin singlet between sites l and m and the latter generates a coherent hopping of the Schwinger bosons. At the mean-field level, the exchange follows as

$$\langle (\vec{S}_l(\vec{x}) \cdot \vec{S}_m(\vec{y}))_{MF} \rangle = |B_{lm}(\vec{x} - \vec{y})|^2 - |A_{lm}(\vec{x} - \vec{y})|^2,$$

with

$$\begin{aligned} A_{lm}^*(\vec{x} - \vec{y}) &= \langle \mathbf{A}_{lm}^\dagger(\vec{x}, \vec{y}) \rangle, \\ B_{lm}^*(\vec{x} - \vec{y}) &= \langle \mathbf{B}_{lm}^\dagger(\vec{x}, \vec{y}) \rangle. \end{aligned}$$

These equations are solved self-consistently taking into account the constraint in the number of bosons $B_{ll}(\vec{R} = \vec{0}) = 4N_c S$, with N_c representing the total number of unit cells and S being the spin strength [26,38].

After solving the mean-field equations on finite but large lattices we primarily extract the extrapolation of the elementary excitation gap Δ . The extrapolation of the gap is performed for system sizes up to 4000 sites following a standard procedure (see, for example, Ref. [26]), but generally, the results for systems bigger than 2000 sites did not show a strong dependence on the size. This gap is used to classify magnetic phases, for which Δ has to be zero. If $\Delta \neq 0$, Bose condensation cannot occur, and the phase is quantum disordered. We can also obtain the real-space spin-correlation function C_l and magnetization m_l [68]. Lattice nematic phases, which preserve the lattice translational invariance but break Z_3 lattice symmetry, came under scrutiny early on in single-layer honeycomb systems. These imply a nonzero order parameter [22,23],

$$\begin{aligned} \rho &= \frac{4}{3} [\langle \vec{S}_1(\vec{r}) \cdot \vec{S}_2(\vec{r}) \rangle + e^{i2\pi/3} \langle \vec{S}_1(\vec{r}) \cdot \vec{S}_2(\vec{r} + \vec{e}_1) \rangle \\ &\quad + e^{i4\pi/3} \langle \vec{S}_1(\vec{r}) \cdot \vec{S}_2(\vec{r} + \vec{e}_2) \rangle]. \end{aligned} \quad (2)$$

Here, we have investigated this order parameter over *all* of the parameter space of Fig. 2(a).

To clarify the procedure we detail our SBMFT results along two paths, (a)–(d) at $J_2 = 0.3$ and (f)–(g) at $J_2 = 0.38$, in a representative part of the phase diagram, depicted in Fig. 2(b). The corresponding evolution of Δ (connected red circles) and ρ (connected black squares) are shown in Figs. 2(c) and 2(d) for the paths (a)–(d) and (f)–(g), respectively. The low-frustration regime (J_2/J_1) was previously studied using SBMFT [26,47].

We start in the light-blue phase around point (a), where Fig. 2(c) features a finite gap and unbroken Z_3 symmetry. This identifies the GSL phase. As J_\perp increases from zero, the gap rapidly decreases and closes *simultaneously* with ρ growing finite. A blowup of this is shown in the top left inset of Fig. 2(c). This behavior is consistent with a spiral phase, which is gapless and breaks Z_3 symmetry. As J_\perp increases further, ρ runs through a maximum and decreases up to a point where $\Delta \neq 0$ again. In stark contrast to the GSL, however, a narrow yellow region of broken Z_3 symmetry *and* gapful behavior surfaces around point (c). This characterizes the lattice nematic phase (VBC2). The top right of Fig. 2(c) shows a blowup of this region. Very different from the VBC1 phase, VBC2 can be found in a much larger range of parameters running all along the upper spiral phase boundary. Finally, entering the blue region around point (d), there is a near-first-order jump to rather large values of Δ where ρ turns zero, restoring Z_3 symmetry. This is consistent with the IDP, adiabatically connecting to the limit of decoupled dimers at $J_\perp = \infty$.

Turning to the second path [points (f) and (g)], it is obvious from Fig. 2(d) that the phase corresponding to point (g) is identical to the corresponding one at point (b). However, different from the GSL at (a), the VBC1 phase around (f) displays behavior of Δ and ρ identical to that of point (c), i.e., a lattice nematic.

In stark contrast to the VBC1 phase, which is rapidly suppressed by the coupling between the planes, the VBC2 phase is induced by combined finite intralayer frustration and interlayer coupling and therefore is associated with the bilayer nature of the system.

IV. SERIES EXPANSION AND BOND-OPERATOR APPROACH

For a complementary analysis of the evolution of the quantum disordered phases, starting from the limit of decoupled dimers, $J_\perp \rightarrow \infty$, we use both series expansion (SE) [69] and bond-operator theory (BOT) [57,70,71]. In BOT, spins at the vertices of each dimer are written as

$$S^\alpha = \left(\pm s^\dagger t_\alpha \pm t_\alpha^\dagger s - \sum_{\beta,\gamma} i \varepsilon_{\alpha\beta\gamma} t_\beta^\dagger t_\gamma \right) / 2,$$

with the constraint

$$s^\dagger s + \sum_{\alpha} t_\alpha^\dagger t_\alpha = 1,$$

where s^\dagger (t_α^\dagger) create singlet (triplet) states of the dimer and $\alpha = 1, 2, 3$ labels the triplet multiplet. BOT maps the spin model onto an interacting Bose gas, for which several schemes of treatment have been proposed [57,70–73]. Here, we use the Holstein-Primakoff (HP) approximation [70,71], where $s^{(\dagger)}$ is replaced by a C number and $s = (1 - \sum_{\alpha} t_\alpha^\dagger t_\alpha)^{1/2}$ is

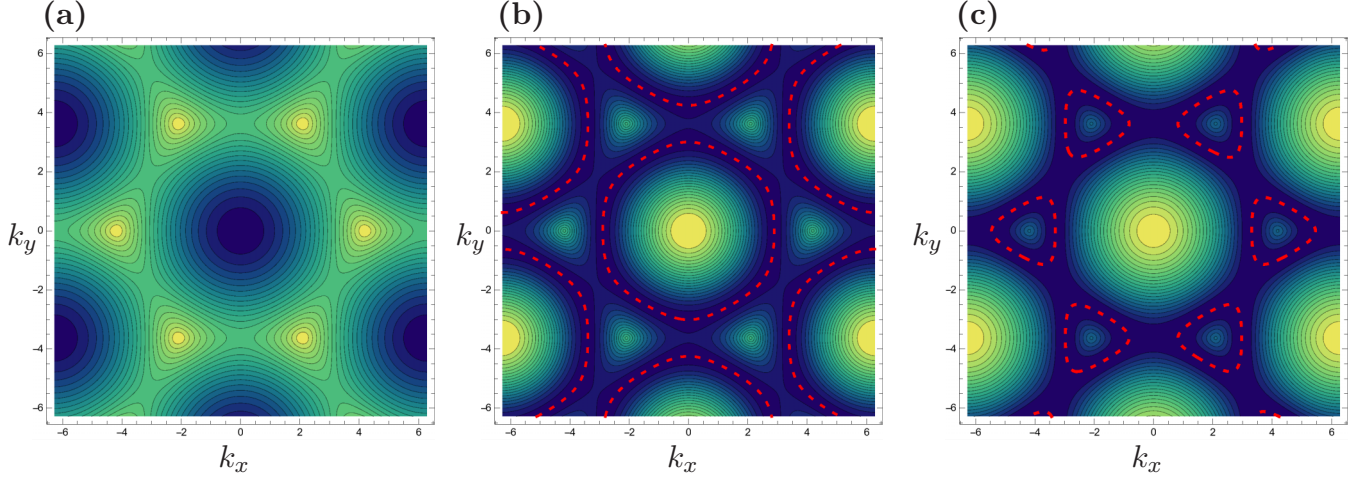


FIG. 3. Contour plot corresponding to the bond-operator boson dispersion close to condensation for (a) $J_2/J_1 = 0.1$, (b) $J_2/J_1 = 0.4$, and (c) $J_2/J_1 = 0.6$. Red dashed lines correspond to curves in the \vec{k} space determining the classical manifold of spiral ground states.

expanded to obtain a quadratic triplon Hamiltonian. Standard Bogoliubov diagonalization yields a ground-state energy per unit cell of

$$E = -\frac{9}{4} + \frac{3}{4N} \sum_{k,\pm} [1 \pm \epsilon_{\pm}(k)]^{1/2},$$

with the triplon dispersions

$$\begin{aligned} \epsilon_{\pm}(k) = & \frac{J_1}{J_{\perp}} [3 + 2 \cos(k_x) + 4 \cos(k_x/2) \cos(\sqrt{3}k_y/2)]^{1/2} \\ & \pm 2 \frac{J_2}{J_{\perp}} [\cos(k_x) + 2 \cos(k_x/2) \cos(\sqrt{3}k_y/2)]. \end{aligned} \quad (3)$$

At $J_1=J_2=0$, for the latter one recovers the bare singlet-triplet gap $\Delta = J_{\perp}$, and for the former $E = -3J_{\perp}/4$, consistent with a bare singlet.

For SE we use the continuous unitary transformation (CUT) method [54,58,74–77] starting from the limit of decoupled dimers. This method allows us to obtain analytical expressions for the ground-state energy and the dispersion of the elementary triplon excitations of the IDP versus $J_{1,2}/J_{\perp}$. We have evaluated these up to $O(4)$. Their rather lengthy expressions are detailed in the Appendix.

In Fig. 2(a) we show the critical lines of the gap closure of the triplon dispersion of the IDP obtained from both BOT-HP (red line) and SE-CUT (blue line). Clearly, comparing them with regions of magnetic ordering obtained from SBMFT, the general trend, i.e., the breakdown of magnetic order versus J_2 and J_{\perp} , is fully consistent with the IDP gap closure. Quantitatively, however, comparing SBMFT and BOT-HP to SE-CUT, the latter predicts a smaller range of stability for semiclassical phases. Since the former two are mean-field theories, such a tendency to prefer ordered phases is a well-known shortcoming. In fact, SE-CUT locates the IDP-Néel transition at $J_{\perp} \simeq 1.6$ for $J_2 = 0$ in Fig. 2(a), in excellent agreement with quantum Monte Carlo calculations [43], and moreover, SE-CUT is rather close to coupled-cluster results for finite, but small, $J_2 \lesssim 0.2$ [48]. For larger J_2 the SE-CUT becomes less reliable, and we are left with only BOT-HP to compare to within the IDP.

Finally, we comment on the location in \vec{k} space of Bose condensation within the BOT-HP compared to the classical magnetic pitch vector \vec{Q} of the bilayer at $S \rightarrow \infty$. As mentioned previously, the latter is independent of J_{\perp} , comprising a Néel state for each plane for $0 < J_2/J_1 < 1/6$ and, for $1/6 < J_2/J_1$, a set of classically degenerate coplanar spiral ground states with

$$\vec{S}_l(\vec{r}) = (-1)^l S [\cos(\vec{Q} \cdot \vec{r} + \theta_l) \hat{i} + \sin(\vec{Q} \cdot \vec{r} + \theta_l) \hat{j}],$$

where the pitch vector lies on the closed curve

$$\begin{aligned} \cos(Q_x) + \cos\left(-\frac{Q_x}{2} + \sqrt{3}\frac{Q_y}{2}\right) \\ + \cos\left(\frac{Q_x}{2} + \sqrt{3}\frac{Q_y}{2}\right) = (J_1/J_2)^2/8 - \frac{3}{2} \end{aligned} \quad (4)$$

and the phase θ_l obeys $\theta_{1,2} = \pi + \theta_{3,4}$ [22]. Comparing this now to the critical wave vector \vec{Q} for Bose condensation within the BOT-HP, we first have $\vec{Q} = (0,0)$, corresponding to a Néel order for $J_2 < \frac{1}{6}$. For $J_2 > \frac{1}{6}$, condensation does not occur at a single point but on lines in \vec{k} space. Remarkably, these are identical to those from the classical states. This is illustrated in Figs. 3(a)–3(c), where we plot contours of the boson dispersion close to condensation at $J_2 = 0.1, 0.4$, and 0.6 and incorporate the degenerate classical spiral pitch vector locations by red dashed lines. In turn, while quantum fluctuations may modify such agreement, it is, nevertheless, interesting to realize that BOT-HP provides some guidance as to the type of semiclassical phase that will emerge upon gap closure.

V. CONCLUSION

In conclusion, the interplay between intralayer frustration and interlayer exchange allows for a rich variety of classical and quantum disordered phases to compete for stability in the bilayer honeycomb antiferromagnet. In this paper, evidence for these phases has been provided over a wide range of coupling constants using three complementary methods, yielding consistent results. Most noteworthy, at intermediate coupling, we have discovered a lattice nematic phase which exists in a region

of parameter space substantially larger than similar phases observed previously in the model at small interlayer coupling. While we have carried out our analysis on a spin-1/2 model, our findings may be relevant for understanding the absence of magnetic order in the spin-3/2 honeycomb bilayer material $\text{Bi}_3\text{Mn}_4\text{O}_{12}(\text{NO}_3)$, where first-principles calculations suggest exchange paths that are identical to our microscopic model and are all of similar magnitude.

ACKNOWLEDGMENTS

C.A.L. gratefully acknowledges the support of NVIDIA Corporation. C.A.L. and M.A. are supported by CONICET (PIP 1691) and ANPCyT (PICT 2013-0009). H.Z. thanks Lu Yu for fruitful discussions and the Institute of Physics, Chinese Academy of Sciences, for financial support. The work of W.B. was supported in part by the DFG through SFB 1143. W.B. also acknowledges the kind hospitality of the PSM, Dresden.

APPENDIX: SERIES EXPANSION

Here, we provide some additional details about the series expansion results presented in this work. The dimer series expansion SE calculations start from the limit of isolated interlayer dimers coupled via J_\perp . For this we decompose the model Hamiltonian of Eq. (1) into

$$H = H_0 + V(J_1, J_2),$$

where H_0 represents decoupled interlayer dimers and $V(J_1, J_2)$ is the interaction part of the Hamiltonian, connecting dimers via on-layer nearest (J_1) and next-nearest (J_2) couplings in units of J_\perp (see Fig. 1).

The spectrum of H_0 is equidistant, which allows us to organize the level structure of H_0 in a block-diagonal form, with

each block labeled by an energy quantum number Q . In this way, $Q = 0$ represents the ground state (*vacuum*), where all dimers are in the singlet state. The $Q = 1$ sector is composed of states obtained by creating one-triplet excitation (*particle*) on a given dimer and so on. The cases in which $Q \geq 2$ represent multiparticle states and are not considered here.

The interacting part of the Hamiltonian $V(J_1, J_2)$ mixes different Q sectors, Losing H , the block diagonal structure of H_0 . However, it is possible to restore the block-diagonal form by application of continuous unitary transformations, using the flow equation method of Wegner [74]. The method can be applied perturbatively, transforming H into a block-diagonal effective Hamiltonian H_{eff} , which has the structure

$$H_{\text{eff}} = H_0 + \sum_{n,m} c_{n,m} J_1^n J_2^m,$$

where $c_{n,m}$ are weighted products of terms in $V(J_1, J_2)$ which conserve the Q number, whose weights are determined by recursive differential equations (see further details in Ref. [58]).

The Q -number conservation allows the direct computation of several observables from H_{eff} in terms of a SE in J_1, J_2 . For the present model we have performed $O(4)$ SE in J_1, J_2 for ground-state energy ($Q = 0$) and for the triplet dispersion ω , i.e., $Q = 1$. Of particular interest for this work is the dispersion since it allows us to delimit the extension of the IDP phase. Note that the dispersion has two branches due to the presence of two dimers per unit cell in the honeycomb lattice. We refer to Ref. [58] for technical details about the calculation. The complete expression for both branches of the dispersion $\omega_\pm(J_1, J_2)$ up to fourth order in J_1, J_2 has the following form:

$$\omega_\pm(J_1, J_2) = \pm a(J_1, J_2) + b(J_1, J_2),$$

where

$$\begin{aligned} a(J_1, J_2) = & 8J_1\sqrt{3 + 2\cos(\alpha_x) + 2\cos(\alpha_x - \alpha_y) + 2\cos(\alpha_y)} - 2J_1^3\cos(\alpha_x - \alpha_y) - 2J_1^3\cos(\alpha_y) + 7J_1^3 \\ & + J_2(5J_1^2 - 2J_1J_2 + 26J_2^2 - 6J_2)\cos(2\alpha_x) - 7J_1^2J_2\cos(\alpha_x - \alpha_y) + 5J_1^2J_2\cos[2(\alpha_x - \alpha_y)] + 10J_1^2J_2\cos(2\alpha_x - \alpha_y) \\ & + 10J_1^2J_2\cos(\alpha_x + \alpha_y) + 10J_1^2J_2\cos(\alpha_x - 2\alpha_y) - 7J_1^2J_2\cos(\alpha_y) + 5J_1^2J_2\cos(2\alpha_y) - 18J_1^2J_2 - 2J_1^2\cos(\alpha_x - \alpha_y) \\ & - 2J_1^2\cos(\alpha_y) + 6J_1^2 - [2J_1^3 + J_1^2(7J_2 + 2) + J_1J_2(9J_2 - 4) + J_2(3J_2^2 + 8J_2 - 8)]\cos(\alpha_x) - 9J_1J_2^2\cos(\alpha_x - \alpha_y) \\ & - 2J_1J_2^2\cos[2(\alpha_x - \alpha_y)] - 4J_1J_2^2\cos(2\alpha_x - \alpha_y) - 4J_1J_2^2\cos(\alpha_x + \alpha_y) - 4J_1J_2^2\cos(\alpha_x - 2\alpha_y) - 9J_1J_2^2\cos(\alpha_y) \\ & - 2J_1J_2^2\cos(2\alpha_y) + 19J_1J_2^2 + 4J_1J_2\cos(\alpha_x - \alpha_y) + 4J_1J_2\cos(\alpha_y) - 4J_1J_2 - 3J_2^3\cos(\alpha_x - \alpha_y) \\ & + 26J_2^3\cos[2(\alpha_x - \alpha_y)] + 5J_2^3\cos[3(\alpha_x - \alpha_y)] + 22J_2^3\cos(2\alpha_x - \alpha_y) + 15J_2^3\cos(3\alpha_x - \alpha_y) + 22J_2^3\cos(\alpha_x + \alpha_y) \\ & + 15J_2^3\cos(2\alpha_x + \alpha_y) + 15J_2^3\cos(\alpha_x + 2\alpha_y) + 22J_2^3\cos(\alpha_x - 2\alpha_y) + 15J_2^3\cos(3\alpha_x - 2\alpha_y) + 15J_2^3\cos(\alpha_x - 3\alpha_y) \\ & + 15J_2^3\cos(2\alpha_x - 3\alpha_y) + 5J_2^3\cos(3\alpha_x) - 3J_2^3\cos(\alpha_y) + 26J_2^3\cos(2\alpha_y) + 5J_2^3\cos(3\alpha_y) - 6J_2^3 - 8J_2^2\cos(\alpha_x - \alpha_y) \\ & - 6J_2^2\cos[2(\alpha_x - \alpha_y)] - 12J_2^2\cos(2\alpha_x - \alpha_y) - 12J_2^2\cos(\alpha_x + \alpha_y) - 12J_2^2\cos(\alpha_x - 2\alpha_y) - 8J_2^2\cos(\alpha_y) \\ & - 6J_2^2\cos(2\alpha_y) + 6J_2^2 + 8J_2\cos(\alpha_x - \alpha_y) + 8J_2\cos(\alpha_y) - 8 \end{aligned}$$

and

$$\begin{aligned} b(J_1, J_2) = & 1 + \frac{1}{128}\{4\cos(\alpha_x)J_1^4 - 10\cos(2\alpha_x)J_1^4 + 4\cos(\alpha_x - \alpha_y)J_1^4 - 10\cos[2(\alpha_x - \alpha_y)]J_1^4 - 20\cos(2\alpha_x - \alpha_y)J_1^4 \\ & + 4\cos(\alpha_y)J_1^4 - 10\cos(2\alpha_y)J_1^4 - 20\cos(\alpha_x + \alpha_y)J_1^4 - 20\cos(\alpha_x - 2\alpha_y)J_1^4 - 87J_1^4 - 432J_2J_1^3 \\ & + 96J_2\cos(\alpha_x)J_1^3 - 32\cos(\alpha_x)J_1^3 + 32J_2\cos(2\alpha_x)J_1^3 + 96J_2\cos(\alpha_x - \alpha_y)J_1^3 - 32\cos(\alpha_x - \alpha_y)J_1^3 \end{aligned}$$

$$\begin{aligned}
& +32J_2 \cos[2(\alpha_x - \alpha_y)]J_1^3 + 64J_2 \cos(2\alpha_x - \alpha_y)J_1^3 + 96J_2 \cos(\alpha_y)J_1^3 - 32 \cos(\alpha_y)J_1^3 + 32J_2 \cos(2\alpha_y)J_1^3 \\
& +64J_2 \cos(\alpha_x + \alpha_y)J_1^3 + 64J_2 \cos(\alpha_x - 2\alpha_y)J_1^3 + 72J_1^3 + 2988J_2^2J_1^2 - 720J_2J_1^2 + 92J_2^2 \cos(\alpha_x)J_1^2 \\
& +64J_2 \cos(\alpha_x)J_1^2 - 32 \cos(\alpha_x)J_1^2 - 364J_2^2 \cos(2\alpha_x)J_1^2 \\
& +48J_2 \cos(2\alpha_x)J_1^2 - 60J_2^2 \cos(3\alpha_x)J_1^2 + 92J_2^2 \cos(\alpha_x - \alpha_y)J_1^2 \\
& +64J_2 \cos(\alpha_x - \alpha_y)J_1^2 - 32 \cos(\alpha_x - \alpha_y)J_1^2 - 364J_2^2 \cos[2(\alpha_x - \alpha_y)]J_1^2 + 48J_2 \cos[2(\alpha_x - \alpha_y)]J_1^2 \\
& -60J_2^2 \cos[3(\alpha_x - \alpha_y)]J_1^2 - 368J_2^2 \cos(2\alpha_x - \alpha_y)J_1^2 + 96J_2 \cos(2\alpha_x - \alpha_y)J_1^2 - 180J_2^2 \cos(3\alpha_x - \alpha_y)J_1^2 \\
& +92J_2^2 \cos(\alpha_y)J_1^2 + 64J_2 \cos(\alpha_y)J_1^2 - 32 \cos(\alpha_y)J_1^2 - 364J_2^2 \cos(2\alpha_y)J_1^2 + 48J_2 \cos(2\alpha_y)J_1^2 - 60J_2^2 \cos(3\alpha_y)J_1^2 \\
& -368J_2^2 \cos(\alpha_x + \alpha_y)J_1^2 + 96J_2 \cos(\alpha_x + \alpha_y)J_1^2 - 180J_2^2 \cos(2\alpha_x + \alpha_y)J_1^2 - 180J_2^2 \cos(\alpha_x + 2\alpha_y)J_1^2 \\
& -368J_2^2 \cos(\alpha_x - 2\alpha_y)J_1^2 + 96J_2 \cos(\alpha_x - 2\alpha_y)J_1^2 - 180J_2^2 \cos(3\alpha_x - 2\alpha_y)J_1^2 - 180J_2^2 \cos(\alpha_x - 3\alpha_y)J_1^2 \\
& -180J_2^2 \cos(2\alpha_x - 3\alpha_y)J_1^2 + 144J_1^2 - 54J_2^4 - 336J_2^3 + 288J_2^2 + 168J_2^4 \cos(\alpha_x) - 128J_2^3 \cos(\alpha_x) - 64J_2^2 \cos(\alpha_x) \\
& +128J_2 \cos(\alpha_x) + 16J_2^4 \cos(2\alpha_x) + 64J_2^3 \cos(2\alpha_x) - 32J_2^2 \cos(2\alpha_x) - 104J_2^4 \cos(3\alpha_x) \\
& +16J_2^3 \cos(3\alpha_x) - 10J_2^4 \cos(4\alpha_x) + 168J_2^4 \cos(\alpha_x - \alpha_y) - 128J_2^3 \cos(\alpha_x - \alpha_y) - 64J_2^2 \cos(\alpha_x - \alpha_y) \\
& +128J_2 \cos(\alpha_x - \alpha_y) + 16J_2^4 \cos[2(\alpha_x - \alpha_y)] + 64J_2^3 \cos[2(\alpha_x - \alpha_y)] - 32J_2^2 \cos[2(\alpha_x - \alpha_y)] \\
& -104J_2^4 \cos[3(\alpha_x - \alpha_y)] + 16J_2^3 \cos[3(\alpha_x - \alpha_y)] - 10J_2^4 \cos[4(\alpha_x - \alpha_y)] + 136J_2^4 \cos(2\alpha_x - \alpha_y) \\
& +32J_2^3 \cos(2\alpha_x - \alpha_y) - 64J_2^2 \cos(2\alpha_x - \alpha_y) - 112J_2^4 \cos(3\alpha_x - \alpha_y) + 48J_2^3 \cos(3\alpha_x - \alpha_y) \\
& -40J_2^4 \cos(4\alpha_x - \alpha_y) + 168J_2^4 \cos(\alpha_y) - 128J_2^3 \cos(\alpha_y) - 64J_2^2 \cos(\alpha_y) + 128J_2 \cos(\alpha_y) + 16J_2^4 \cos(2\alpha_y) \\
& +64J_2^3 \cos(2\alpha_y) - 32J_2^2 \cos(2\alpha_y) - 104J_2^4 \cos(3\alpha_y) + 16J_2^3 \cos(3\alpha_y) - 10J_2^4 \cos(4\alpha_y) \\
& +136J_2^4 \cos(\alpha_x + \alpha_y) + 32J_2^3 \cos(\alpha_x + \alpha_y) - 64J_2^2 \cos(\alpha_x + \alpha_y) - 60J_2^4 \cos[2(\alpha_x + \alpha_y)] - 112J_2^4 \cos(2\alpha_x + \alpha_y) \\
& +48J_2^3 \cos(2\alpha_x + \alpha_y) - 40J_2^4 \cos(3\alpha_x + \alpha_y) - 112J_2^4 \cos(\alpha_x + 2\alpha_y) + 48J_2^3 \cos(\alpha_x + 2\alpha_y) + 136J_2^4 \cos(\alpha_x - 2\alpha_y) \\
& +32J_2^3 \cos(\alpha_x - 2\alpha_y) - 64J_2^2 \cos(\alpha_x - 2\alpha_y) - 60J_2^4 \cos[2(\alpha_x - 2\alpha_y)] - 112J_2^4 \cos(3\alpha_x - 2\alpha_y) \\
& +48J_2^3 \cos(3\alpha_x - 2\alpha_y) - 60J_2^4 \cos(4\alpha_x - 2\alpha_y) \\
& -112J_2^4 \cos(\alpha_x - 3\alpha_y) + 48J_2^3 \cos(\alpha_x - 3\alpha_y) - 112J_2^4 \cos(2\alpha_x - 3\alpha_y) \\
& +48J_2^3 \cos(2\alpha_x - 3\alpha_y) - 40J_2^4 \cos(4\alpha_x - 3\alpha_y) \\
& -40J_2^4 \cos(\alpha_x - 4\alpha_y) - 40J_2^4 \cos(3\alpha_x - 4\alpha_y) - 40J_2^4 \cos(\alpha_x + 3\alpha_y)\},
\end{aligned}$$

in which α are related to the k reciprocal lattice vectors by $\alpha_x = \frac{\sqrt{3}}{2}k_x + \frac{3}{2}k_y$ and $\alpha_y = -\frac{\sqrt{3}}{2}k_x + \frac{3}{2}k_y$.

The triplet gap $\Delta_{\pm}(J_1, J_2)$, that is, the minimum of the two dispersion branches $\omega_{\pm}(J_1, J_2)$ along the range presented in this work, is given by

$$\begin{aligned}
\Delta_{\pm}(J_1, J_2) = & -\frac{165J_1^4}{128} + \frac{9J_1^3J_2}{8} - \frac{3J_1^3}{16} - \frac{3J_1^2J_2^2}{2} - \frac{3J_1^2J_2}{4} + \frac{3J_1^2}{8} - \frac{33J_2^4}{8} - \frac{3J_2^3}{4} - \frac{3J_2^2}{2} + 3J_2 \\
& \pm \left| -\frac{3J_1^4}{16} - \frac{9J_1^3J_2}{8} + \frac{39J_1^2J_2^2}{8} - \frac{3J_1^2J_2}{2} - \frac{351J_1J_2^3}{8} + \frac{27J_1J_2^2}{2} - \frac{9J_1J_2}{2} + \frac{3J_1}{2} \right| + 1. \quad (A1)
\end{aligned}$$

Finally, the critical line in the plane J_2 - J_{\perp} presented in Fig. 2(a) of the main text (blue line) was then obtained by numerically

solving $\Delta_{\pm}(1/J_{\perp}, J_2/J_{\perp}) = 0$ since the unit in the main text is J_1 and not J_{\perp} as presented here.

[1] R. Moessner and A. P. Ramirez, *Phys. Today* **59**(2), 24 (2006).

[2] L. Balents, *Nature (London)* **464**, 199 (2010).

[3] X.-G. Wen, *Int. J. Mod. Phys. B* **4**, 239 (1990).

[4] X.-G. Wen, *Phys. Rev. B* **65**, 165113 (2002).

[5] A. Kitaev, *Ann. Phys. (NY)* **303**, 2 (2003).

[6] S. Benjamin and J. Kelly, *Nat. Mater.* **14**, 561 (2015).

[7] D. Ristè, S. Poletto, M.-Z. Huang, A. Bruno, V. Vesterinen, O.-P. Saira, and L. DiCarlo, *Nat. Commun.* **6**, 7983 (2015).

[8] A. D. Córcoles, E. Magesan, S. J. Srinivasan, A. W. Cross, M. Steffen, J. M. Gambetta, and J. M. Chow, *Nat. Commun.* **6**, 7979 (2015).

[9] M. E. Zhitomirsky, *Phys. Rev. B* **67**, 104421 (2003).

- [10] S. Pakhira, C. Mazumdar, R. Ranganathan, and M. Avdeev, *Nat. Sci. Rep.* **7**, 7367 (2017).
- [11] K. Kim, M.-S. Chang, S. Korenblit, R. Islam, E. E. Edwards, J. K. Freericks, G.-D. Lin, L.-M. Duan, and C. Monroe, *Nature (London)* **465**, 590 (2010).
- [12] J. Struck, C. Ölschläger, R. L. Targat, P. Soltan-Panahi, A. Eckardt, M. Lewenstein, P. Windpassinger, and K. Sengstock, *Science* **333**, 996 (2011).
- [13] G. 't Hooft, *Nucl. Phys. B* **79**, 276 (1974).
- [14] C. Castelnovo, R. Moessner, and S. L. Sondhi, *Nature (London)* **451**, 42 (2008).
- [15] E. Mengotti, L. J. Heyderman, A. F. Rodríguez, F. Nolting, R. V. Hügeli, and H.-B. Braun, *Nat. Phys.* **7**, 68 (2011).
- [16] L. D. C. Jaubert, M. Haque, and R. Moessner, *Phys. Rev. Lett.* **107**, 177202 (2011).
- [17] D. Austin, E. J. Copeland, and R. J. Rivers, *Phys. Rev. D* **49**, 4089 (1994).
- [18] L. Savary and L. Balents, *Rep. Prog. Phys.* **80**, 016502 (2017).
- [19] K. Matan, T. Ono, Y. Fukumoto, T. J. Sato, J. Yamaura, M. Yano, K. Morita, and H. Tanaka, *Nat. Phys.* **6**, 865 (2010).
- [20] D. Grohol, K. Matan, J.-H. Cho, S.-H. Lee, J. W. Lynn, D. G. Nocera, and Y. S. Lee, *Nat. Mater.* **4**, 323 (2005).
- [21] K. Damle and T. Senthil, *Phys. Rev. Lett.* **97**, 067202 (2006).
- [22] A. Mulder, R. Ganesh, L. Capriotti, and A. Paramekanti, *Phys. Rev. B* **81**, 214419 (2010).
- [23] S. Okumura, H. Kawamura, T. Okubo, and Y. Motome, *J. Phys. Soc. Jpn.* **79**, 114705 (2010).
- [24] F. Wang, *Phys. Rev. B* **82**, 024419 (2010).
- [25] H. Mosadeq, F. Shahbazi, and S. Jafari, *J. Phys.: Condens. Matter* **23**, 226006 (2011).
- [26] D. C. Cabra, C. A. Lamas, and H. D. Rosales, *Phys. Rev. B* **83**, 094506 (2011).
- [27] R. Ganesh, D. N. Sheng, Y.-J. Kim, and A. Paramekanti, *Phys. Rev. B* **83**, 144414 (2011).
- [28] A. F. Albuquerque, D. Schwandt, B. Hetényi, S. Capponi, M. Mambrini, and A. M. Läuchli, *Phys. Rev. B* **84**, 024406 (2011).
- [29] B. K. Clark, D. A. Abanin, and S. L. Sondhi, *Phys. Rev. Lett.* **107**, 087204 (2011).
- [30] D. Cabra, C. Lamas, and H. Rosales, *Mod. Phys. Lett. B* **25**, 891 (2011).
- [31] F. Mezzacapo and M. Boninsegni, *Phys. Rev. B* **85**, 060402(R) (2012).
- [32] R. F. Bishop, P. H. Y. Li., D. J. J. Farnell, and C. E. Campbell, *J. Phys.: Condens. Matter* **24**, 236002 (2012).
- [33] P. H. Y. Li, R. F. Bishop, D. J. J. Farnell, and C. E. Campbell, *Phys. Rev. B* **86**, 144404 (2012).
- [34] R. F. Bishop, P. H. Y. Li, D. J. J. Farnell, and C. E. Campbell, *J. Phys.: Condens. Matter* **25**, 306002 (2013).
- [35] S.-S. Gong, D. N. Sheng, O. I. Motrunich, and M. P. A. Fisher, *Phys. Rev. B* **88**, 165138 (2013).
- [36] R. Ganesh, J. van den Brink, and S. Nishimoto, *Phys. Rev. Lett.* **110**, 127203 (2013).
- [37] Z. Zhu, D. A. Huse, and S. R. White, *Phys. Rev. Lett.* **110**, 127205 (2013).
- [38] H. Zhang and C. A. Lamas, *Phys. Rev. B* **87**, 024415 (2013).
- [39] F. Ferrari, S. Bieri, and F. Becca, *Phys. Rev. B* **96**, 104401 (2017).
- [40] O. Smirnova, M. Azuma, N. Kumada, Y. Kusano, M. Matsuda, Y. Shimakawa, T. Takei, Y. Yonesaki, and N. Kinomura, *J. Am. Chem. Soc.* **131**, 8313 (2009).
- [41] H. C. Kandpal and J. van den Brink, *Phys. Rev. B* **83**, 140412 (2011).
- [42] M. Matsuda, M. Azuma, M. Tokunaga, Y. Shimakawa, and N. Kumada, *Phys. Rev. Lett.* **105**, 187201 (2010).
- [43] R. Ganesh, S. V. Isakov, and A. Paramekanti, *Phys. Rev. B* **84**, 214412 (2011).
- [44] J. Oitmaa and R. R. P. Singh, *Phys. Rev. B* **85**, 014428 (2012).
- [45] H. Zhang, M. Arlego, and C. A. Lamas, *Phys. Rev. B* **89**, 024403 (2014).
- [46] M. Arlego, C. A. Lamas, and H. Zhang, *J. Phys.: Conf. Ser.* **568**, 042019 (2014).
- [47] H. Zhang, C. A. Lamas, M. Arlego, and W. Brenig, *Phys. Rev. B* **93**, 235150 (2016).
- [48] R. F. Bishop and P. H. Y. Li, *Phys. Rev. B* **95**, 134414 (2017).
- [49] T. Krokhmalkii, V. Baliha, O. Derzhko, J. Schulenburg, and J. Richter, *Phys. Rev. B* **95**, 094419 (2017).
- [50] I. Bose, *Phys. Rev. B* **45**, 13072 (1992).
- [51] I. Bose and S. Gayen, *Phys. Rev. B* **48**, 10653(R) (1993).
- [52] A. Honecker, F. Mila, and M. Troyer, *Eur. Phys. J. B* **15**, 227 (2000).
- [53] W. Brenig and K. W. Becker, *Phys. Rev. B* **64**, 214413 (2001).
- [54] M. Arlego and W. Brenig, *Eur. Phys. J. B* **53**, 193 (2006).
- [55] C. A. Lamas and J. M. Matera, *Phys. Rev. B* **92**, 115111 (2015).
- [56] J. M. Matera and C. A. Lamas, *J. Phys.: Condens. Matter* **26**, 326004 (2014).
- [57] S. Sachdev and R. N. Bhatt, *Phys. Rev. B* **41**, 9323 (1990).
- [58] C. Knetter and G. S. Uhrig, *Eur. Phys. J. B* **13**, 209 (2000).
- [59] A. Auerbach and D. P. Arovas, *Phys. Rev. Lett.* **61**, 617 (1988).
- [60] A. Auerbach, *Interacting Electrons and Quantum Magnetism* (Springer, New York, 1994).
- [61] A. Auerbach and D. P. Arovas, in *Introduction to Frustrated Magnetism* (Springer, Berlin, 2011), Chap. 7, p. 70.
- [62] H. A. Ceccatto, C. J. Gazza, and A. E. Trumper, *Phys. Rev. B* **47**, 12329 (1993).
- [63] A. E. Trumper, L. O. Manuel, C. J. Gazza, and H. A. Ceccatto, *Phys. Rev. Lett.* **78**, 2216 (1997).
- [64] R. Flint and P. Coleman, *Phys. Rev. B* **79**, 014424 (2009).
- [65] A. Mezio, C. Sposetti, L. Manuel, and A. Trumper, *Eur. Phys. Lett.* **94**, 47001 (2011).
- [66] L. Messio, B. Bernu, and C. Lhuillier, *Phys. Rev. Lett.* **108**, 207204 (2012).
- [67] L. Messio, C. Lhuillier, and G. Misguich, *Phys. Rev. B* **87**, 125127 (2013).
- [68] For the use of correlations and staggered magnetization to classify magnetic phases see, for example, Ref. [26].
- [69] J. Oitmaa, C. Hamer, and W. Zheng, *Series Expansion Methods for Strongly Interacting Lattice Models* (Cambridge University Press, Cambridge, 2006).
- [70] A. V. Chubukov, *JETP Lett.* **49**, 129 (1989).
- [71] A. V. Chubukov and T. Jolicoeur, *Phys. Rev. B* **44**, 12050(R) (1991).
- [72] V. N. Kotov, O. Sushkov, Zheng Weihong, and J. Oitmaa, *Phys. Rev. Lett.* **80**, 5790 (1998).
- [73] M. Matsumoto, B. Normand, T. M. Rice, and M. Sigrist, *Phys. Rev. Lett.* **89**, 077203 (2002).
- [74] F. Wegner, *Ann. Phys. (Berlin, Ger.)* **506**, 77 (1994).
- [75] M. Arlego and W. Brenig, *Phys. Rev. B* **84**, 134426 (2011).
- [76] M. Arlego and W. Brenig, *Phys. Rev. B* **78**, 224415 (2008).
- [77] M. Arlego and W. Brenig, *Phys. Rev. B* **75**, 024409 (2007).